Aerodynamic Study and Mechanization Concepts for Flapping-Wing Micro Aerial Vehicles

Maglasang, Jonathan
Department of Aeronautics and Astronautics : Graduate Student

Isogai, Koji
Department of Aerospace Engineering, Nippon Bunri University : Professor

Goto, Norihiro
Department of Aeronautics and Astronautics : Professor

Yamasaki, Masahide
Department of Aeronautics and Astronautics : Research Associate

出版情報：九州大学工学紀要. 66 (1), pp.71-82, 2006-03. 九州大学大学院工学研究院
バージョン：
権利関係：

Memoirs of the Faculty of Engineering, Kyushu University, Vol.66, No.1, March 2006

Aerodynamic Study and Mechanization Concepts for Flapping-Wing Micro Aerial Vehicles

by

Jonathan MAGLASANG[*], Koji ISOGAI[**] , Norihiro GOTO[***]
and Masahide YAMASAKI[†]

(Received February 20, 2006)

Abstract

In order to investigate the feasibility of a highly efficient flapping system that is capable of avian maneuvers such as rapid takeoff, hover and gliding, numerical and experimental studies have been conducted on the flapping wing kinematics and aerodynamics, and on the mechanization and design requirements for a bird-like micro aerial vehicle (MAV). An unsteady viscous flow simulation has been performed using a 3D Navier-Stokes code in investigating the effects of dynamic stall phenomenon on the propulsive efficiency, thrust, and lift of the flapping wing. A mechanical flapping-wing micro aerial vehicle that utilizes both the flapping and feathering characteristics of a typical pigeon (*Columba livia*) has been successfully constructed, and has indicated excellent aerodynamic performance during preliminary wind tunnel testing. The flapping-feathering mechanism employed in this MAV model has been synthesized and constructed so as to best describe the properly coordinated flapping and feathering motions of the wing at an optimum phase angle difference of 90^{o} in a horizontal steady level flight condition.

Keywords: Micro aerial vehicle, Flapping-wing, Propulsive efficiency

1. Introduction

The development of extremely small aerial robots or micro aerial vehicles (MAVs) of the same range in size and weight as natural fliers has sparked renewed interest in flapping flight because of their unique capability to perform a wide array of missions such as over-the-hill reconnaissance and surveillance, targeting, tagging, bio-chemical sensing, and flying in a rarefied atmosphere such as on Mars. With a size of approximately 15 cm in length, width or height and a flight speed of a few

[*] Graduate Student, Department of Aeronautics and Astronautics
[**] Professor, Department of Aerospace Engineering, Nippon Bunri University
[***] Professor, Department of Aeronautics and Astronautics
[†] Research Associate, Department of Aeronautics and Astronautics

meters per second, a micro aerial vehicle (MAV) will fly at Reynolds number (10^4-10^5) far lower than for conventional aircraft (10^8). In this low Reynolds number flight regime, MAV aerodynamic behavior is different from that of the larger, faster aircraft, because viscous forces are more significant when we get down to this size and air speed range. Despite recent remarkable achievements obtained with fixed and rotary UAVs, their use in many tasks is still limited by their maneuverability and size. In order to overcome these limitations, the extraordinary flight capabilities of birds and insects have inspired the design of extremely small aerial robots or MAVs with flapping wings mimicking real flying insects and birds. An aerial vehicle with this design is generally scalable up to a size on the order of few millimeters as can be observed in nature.

Based on several studies conducted on many different families of insects and birds, biologists and naturalists have provided the kinematic descriptions of flapping wing motion and empirical correlations between flapping frequency, weight, wing span, and power requirements, while biofluid-dynamicists have provided the explanation of the underlying physical phenomena both in the quasi-steady limit and in the fully unsteady flow regime[1) - 9)]. Computational Fluid Dynamics (CFD) has been used recently to investigate the unsteady flow phenomena in oscillating wings to validate different aerodynamic models and to shed light to phenomena underlying flapping flight. Jones and Platzer[10)] have made their contributions by calculating the inviscid flow for 2D airfoils in plunging and pitching motion in comparison with analytical results. Calculations of the inviscid 3D flow around flapping wings are also available with respect to time-dependent forces in the works of Smith[11)], and Vest and Katz[12)], but results for mean thrust output and efficiency are rarely available. For the viscous flow around 2D and 3D wings, Navier-Stokes solutions have been presented by Isogai et al[13)] and Isogai[14)], respectively.

Another major advantage to flapping-wing design relates to the minimum speed of the vehicle that allows longer target coverage and its ability to perform short takeoffs and landing. Provided with enough power and sophisticated control system, a vehicle with flapping wings could actually takeoff and land vertically.

Unfortunately, because of the mechanical and aerodynamic complexities inherent in flapping flight, flapping-wing design and construction have thus far caused present biomimicked MAVs to be only moderately successful. In this paper, the flapping-wing kinematics and aerodynamics, and the mechanization concepts and design requirements for a bird-like MAV are discussed.

2. The Flapping Wing Motion

2.1 General flapping wing kinematics

In general, there are four degrees of freedom in each wing that are used to achieve flight in nature: flapping, lagging, feathering, and spanning. *Flapping* is an angular movement of the wing about an axis in the direction of flight. *Lagging* is an angular movement of the wing about a vertical axis which effectively moves the wing forward and backward parallel to the body. *Feathering* is an angular movement about an axis in the wing which tilts the wing to change its angle of attack. *Spanning* is an expanding and contracting of the wingspan. These motions somehow require a universal joint similar to the shoulder of a human being. But not all flying animals implement all of these motions. Most insects for instance do not use the spanning technique. Thus, flapping flight is possible with possible few combinations of these four degrees of freedom.

Flapping flight is actually possible with only one degree of freedom by using “flapping” alone. Several studies have been made on flapping flight using this one degree of freedom. Vest and Katz[15)] pointed out that one-degree of freedom flapping MAV, modeled after a typical pigeon (*Columba livia*), can develop sufficient thrust to propel itself in a steady forward flight. It was also

proposed that the propulsive efficiency of a future MAV in a steady forward flight can be significantly improved by adding periodic twist (feathering) during the flapping cycle.

Of the four degrees of freedom available in flapping flight in nature, it is the combination of the flapping and feathering motions that makes the most significant contribution to the lift and thrust production. It is therefore practical to just utilize these two degrees of freedom in designing and building an effective bird-like MAV. Using these two degrees of freedom there are four important variables with respect to wing kinematics: (1) wing beat frequency, (2) wing beat amplitude, (3) wing feathering as a function of wing position, and (4) stroke plane angle. When properly coordinated, these motions can provide lift not only during downstroke, but also during upstroke. The ability to generate lift on both strokes leads to the potential for hovering flight in insect-like (entomopter) and bird-like (ornithopter) micro aerial vehicle.

2.2 Coupled flapping-feathering motion

With the aid of the analysis of the flow around a 2D airfoil in a combined plunging and pitching motion, the kinematics of the coupled flapping and feathering motion could be well established as described in **Fig.1**.

The flapping angle, θ (the angle of inclination against the horizontal X-Y plane), and the feathering or pitching angle, α, and the plunging position, z, are given by the following relationships,

$$\theta(t) = \theta_o \cos(2\pi ft), \tag{1}$$

$$\alpha(t) = \alpha_o + \alpha_1 \cos(2\pi ft + \phi), \tag{2}$$

$$z(t) = z_l \cos(2\pi ft), \tag{3}$$

where f is the oscillation frequency, φ is the phase angle, and α_o is the mean angle of attack.

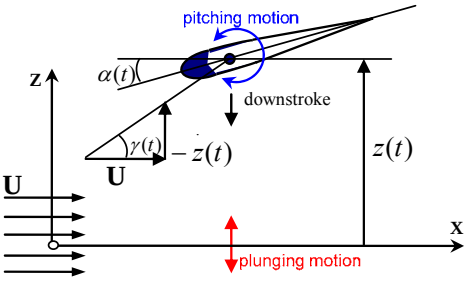

Fig. 1 Coupled plunging and pitching motion.

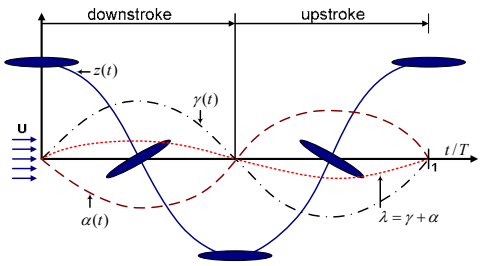

Fig. 2 Motion coordination by phase angle.

The pitching motion defined in Eq. (2) consists of a time-dependent part with amplitude α_l. The momentary pitching angle $\alpha(t)$ is counted from the horizontal parallel to the X-axis and the pitching motion can vary in phase φ relative to the plunging motion. The oscillation frequency f is most often expressed in non-dimensional form as the reduced frequency (k),

$$k = \frac{\pi fc}{U_\infty}, \tag{4}$$

where U_∞ is the free stream velocity and c is the chord length. The reduced frequency, together with the dimensionless plunging amplitude (z_l/c), influences the angle of attack (γ) caused by pure

plunging as shown in the figure and is given by,

$$\gamma(t) = \tan^{-} \frac{-\dot{z}(t)}{U_{\infty}}. \tag{5}$$

The maximum angle of attack through pure plunging for small values of k and z_l/c is approximately,

$$\gamma_l \approx 2kz_l/c, \tag{6}$$

where $\gamma_l \approx \tan^{-}(\gamma)$.

The momentary effective angle of attack, $\lambda\ (\gamma \pm \alpha)$, can be enlarged or diminished depending on the phase shift φ of the superimposed pitching motion in Eq. (2), and shown in **Fig.2** where the phase angle $\varphi = 90^o$. In order to ensure attached flow throughout the entire flapping cycle, λ is to be kept below 12^o to 15^o.

2.3 Basic aerodynamics

A flapping wing generates lift and thrust mainly by virtue of the so-called Knoller-Betz effect[16), 17)], that is, the wing oscillations induce vertical lift force and longitudinal thrust force components of the aerodynamic force (the force normal to the direction of the free stream velocity relative to the flapping wing), and by the complex effects of the generated vortex structures which enable high lifting and propulsive properties. Lift and thrust generation can be increased by increasing the flapping amplitude or the flapping frequency as long as the flow remains attached to the airfoil. The aerodynamic lift, drag, and thrust coefficients can be expressed as follows:

$$C_L = \frac{L}{\frac{1}{2}\rho U^2 S}, \qquad C_D = \frac{D}{\frac{1}{2}\rho U^2 S}, \qquad C_T = \frac{T}{\frac{1}{2}\rho U^2 S}, \tag{7}$$

where L, D, T, U, S, and ρ are lift, drag, thrust, flight speed, wing planform area, and air density, respectively. In steady level flight, the lift force equals the body weight, W_g, and so the wing loading can be expressed as

$$L = W_g = \frac{1}{2}\rho U^2 S C_L \Rightarrow W_g/S = \frac{1}{2}\rho U^2 C_L. \tag{8}$$

The wing loading summarizes the opposing action between two classes of forces in flight: (1) the gravitational and inertial forces, and (2) the aerodynamic forces that are responsible for creating lift and thrust. The range of wing loading is limited by physical constraints. As an example, larger birds do not have high flapping frequency since their bones can not withstand the stresses imposed by moving such a large inertial load.

Another important parameter in forward flight is the reduced frequency, k, which is a measure of the degree of unsteadiness and is given earlier in Eq. (4). The reduced frequency is simply a comparison of the angular velocity and the flow speed. As k increases, so does the flow unsteadiness. $k = 0$ corresponds to a rigid fixed-wing vehicle, while the normal cruising flight of a typical pigeon has $k = 0.25$.

2.4 The power muscle

Depending on the characteristics of the wings and body and its flight speed, flapping-wing design requires a certain amount of power to remain aloft in still air. In birds for instance, the

pectoralis-major muscle which is entirely responsible for the heavily loaded downstroke (*15%* of the total mass), the *supracoracoideus* muscle which powers the upstroke, and the tail muscles (*levator caudae* and *depressor caudae*) are taking up a proportion of about *20%* of an animal's total mass.

For birds, Weis-Fogh[18] set the upper limit on the sustained power that can be generated per unit mass of muscle at *200 W per kg of muscle* (for *man*: *15-20 W per kg of muscle*). Given the proportion that a maximum of *20%* of an animal's total mass is taken up by the flight muscle, the greatest sustainable specific power in flapping forward flight is *40 W/kg*, with some possible reduction below that value as size increases. Pennycuick[19] suggested further that the upper limit on mass may be about *12 kg*, and that above this value the animal can no longer sustain the output needed for flapping flight.

The power requirement of an MAV depends on (1) weight of the vehicle, (2) flight speed, and (3) aerodynamic parameter (C_L/C_D). As the size of the MAV reduces, the weight becomes lighter. However, the small physical size and low flight speed also result in substantially lower Reynolds number, which causes C_L/C_D to decrease. This degradation in aerodynamic performance means that an MAV can not simply be designed based on the same concept as the conventional aircraft, for otherwise it lacks aerodynamic characteristics to remain airborne.

In a steady level flight, the average power output is determined by multiplying the average thrust with the flight speed,

$$\overline{P_{out}} = \overline{T}U \,. \tag{9}$$

The propulsive efficiency, η_P, for one flapping cycle, is an essential parameter since it measures how well the input power, P_{in}, is transformed to output power, P_{out}, and is given by

$$\eta_P = \frac{P_{out}}{P_{in}} \,. \tag{10}$$

The following formulas given by Rayner and Gordon[20] for birds in continuous vortex wake model make it possible to estimate the power-to-mass ratio for birds or for machines that can attain performance comparable to birds:

Maximum Range Speed

$$V_{mr}(m/s) = 10.00 M^{0.413} B^{-0.553} S^{-0.095} \tag{11}$$

Mechanical Power at that Speed

$$P_{mr}(W) = 27.21 M^{1.590} B^{-1.818} S^{0.275} \tag{12}$$

Total Power

$$P_{met}(W) = 114.61 M^{1.145} B^{-1.225} S^{0.523} \tag{13}$$

where M = mass (*kg*), B = wingspan (*m*), and S = wing planform area (m^2). The total power for flight in a bird is measured as the total rate of metabolic energy uptake P_{met}.

A sample calculation for a typical pigeon whose data are listed in **Table 1** shows that V_{mr} = *11.02 m/s*, P_{mr} = *6.03 W*, and P_{met} = *15.15 W*.

Since a bird controls speed by varying its wingbeat kinematics, and that the wingbeat frequency and amplitude are directly related to muscle contraction rate, and that the muscle efficiency is related to muscle strain rate, it is quite difficult to predict the physiological efficiency since it varies with the flight speed. However, these constraints on efficiency may not be important

for an MAV if the actuator(s) responsible for wing movement can maintain efficiency while varying wingbeat kinematics appropriately.

3. Numerical Simulation

As far as the three-dimensional (3D) wing is concerned, all the previous theoretical studies were based on the potential flow assumption. However, as we can see in flying birds, the amplitude of the flapping motion of the wing is very large (for example, the flapping angle of a pigeon is about $\pm 50^o$ as listed in **Table 1**) that the induced angle of attack (due to the flapping motion of the wing) exceeds easily the stalling angle. Thus, in the present study, a 3D compressible Navier-Stokes code is used in order to evaluate the unsteady viscous flow around the flapping pigeon (*Columba livia*) wing and the role of the flow separation, especially the effect of dynamic stall on the propulsive efficiency, thrust, and lift of the flapping wing being investigated.

There are two major reasons for the employment of pigeon in this research, namely, (1) its availability, and (2) because this specie has been used in the past by other investigators, either for experimentation (Pennycuick[21]) or for theoretical analysis (Vest and Katz[22]). The pigeon wing plan form, wing section, and the geometrical twist distribution measured by Nachtigall and Wieser[23] are being used and shown in **Fig.3**. The detailed values of the wing geometry and the typical pigeon characteristics in a steady level flight are shown in **Table 1**. The pitching amplitude value is taken at 75% semi-span station. The data listed in **Table 1** and the aerodynamic performance results obtained from the numerical simulations are used as inputs in the design and development of the pigeon-like MAV.

Table 1 Typical pigeon characteristic being used.

Aspect ratio = 7.2	Flapping frequency = 8Hz
Wing span = 0.66 m	Reduced frequency = 0.25
Wing area = 0.062 m^2	Flapping amplitude = $\pm 50^o$
Wing chord = 0.11 m	Pitching amplitude = $\pm 30^o$
Body mass = 0.39 kg	Phase difference = 90^o
Tail length = 0.12 m	Air speed = 11 m/s
Tail area = 0.01 m^2	

The grid used in the computation is C-H type structured grid, 240 (chordwise) x 31 (normal to surfaces) x 19 (spanwise). In the computations, Mach number and Reynolds number are assumed to be 0.30 and 10^5, respectively, and Baldwin and Lomax's[24] algebraic turbulence model is employed.

The numerical simulation results showed that the propulsive efficiency, $n_p = 0.42$, thrust coefficient $C_T = 0.12$, and lift coefficient $C_L = 0.72$. Vest and Katz[22] have computed the same case by using panel method, obtaining $n_p = 0.64$, thrust coefficient $C_T = 0.13$, and lift coefficient $C_L = 0.85$. In this study's computations, the large scale flow separation is observed on the upper surface from 70% semispan to the tip station at the instant of $kt = \pi$ when the induced angle of attack becomes maximum. Since the occurrence of the flow separation reduces the propulsive efficiency considerably, the results obtained in this present study seem to be quite reasonable compared with those obtained by Vest and Katz[22] using the panel method.

Figure 4 shows the flow pattern around the flapping pigeon wing, and **Fig.5** shows the variation of lift (L), thrust (T) and rate of work (W) during one cycle of oscillation. It can be seen that most of the lift and thrust are generated during the downstroke process ($kt = \pi/2 - 3/2\pi$).

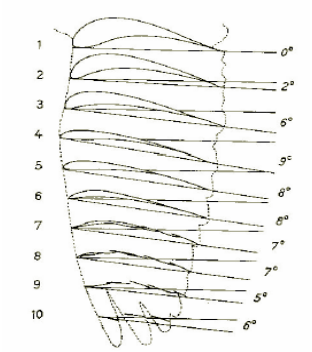

Fig. 3 Pigeon wing from Ref. 23).

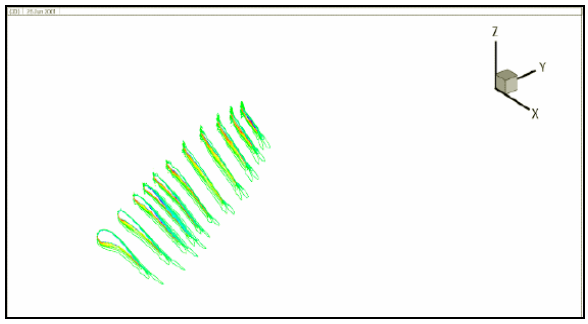

Fig. 4 Flow pattern around the pigeon's wing.

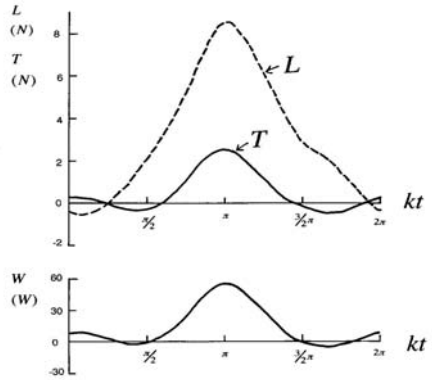

Fig. 5 Variation of lift, thrust and rate of work.

4. Mechanization Concepts

4.1 The flapping-feathering mechanism

The flapping motion of the wing is described by a planar four-bar mechanical linkage (**Fig.6.a**), while the feathering motion is described by a modified five-bar linkage (**Fig.6.b**) which can be highly approximated by an equivalent planar four-bar mechanical linkage in the synthesis. These two mechanical linkages are interconnected to form a set of flapping-feathering mechanism to produce a properly coordinated flapping and feathering motion of the wing for an entire flapping cycle. The insertion of joint *C* in the feathering mechanism allows links *EC* and O_4C to have additional degree of freedom in a moving plane determined by the position of the link O_4B of the flapping mechanism that eventually allows the smooth motion of the two interconnected mechanisms. The flapping-feathering mechanism has been designed to have the same upstroke and downstroke period throughout the entire flapping cycle for a constant crank (O_2A) angular speed input.

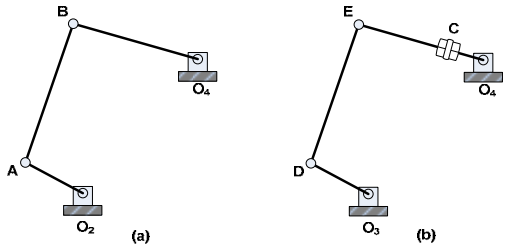

Fig. 6 (a) The flapping, and (b) feathering mechanisms.

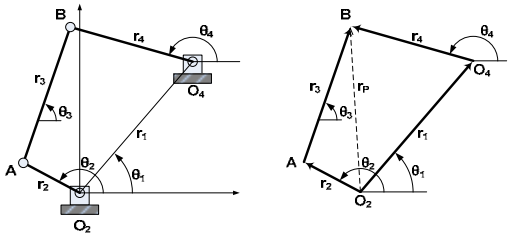

Fig. 7 Schematic of the four-bar mechanical linkage.

In the flapping and feathering mechanism (four-bar crank-rocker), the crank (input), r_2, rotates for 360°, and the rocker (output), r_4, oscillates through an angle θ_4 as shown in **Fig.7** and **Fig.8**. Link r_3 is called the coupler and r_1 is the rigid frame link. The loop closure equation of the vector polygon in **Fig.7** is given by,

$$\vec{r}_2 + \vec{r}_3 = \vec{r}_P = \vec{r}_1 + \vec{r}_4, \tag{14}$$

and by utilizing Euler's equation it becomes,

$$\begin{aligned} r_2 e^{j\theta_2} + r_3 e^{j\theta_3} &= r_1 e^{j\theta_1} + r_4 e^{j\theta_4}; \\ e^{j\theta} &= \cos\theta + j\sin\theta. \end{aligned} \tag{15}$$

The linkage instantaneous position is obtained and given in Eqs. (16) to (19). The velocity and acceleration equations can be obtained by taking the first and second time derivatives of Eq. (15), as shown in Eqs. (20) to (21) and Eqs. (22) to (24), respectively. **Figure 8** shows the graph of the motion of the four-bar mechanical linkage described above with $r_1 = 0.4$, $r_2 = 0.2$, $r_3 = 0.363$, $r_4 = 0.261$, $\theta_1 = 65.2^o$, and with a constant crank input speed of *64.2 rad/sec*. The flapping wing is attached to the rocker (r_4) of the flapping mechanism and to the rocker (r_4) of the feathering mechanism. **Figure 9** shows the schematic of the flapping-wing MAV model with the flapping-feathering mechanism.

Position:

$$\begin{aligned} A &= 2r_1 r_4 \cos\theta_1 - 2r_2 r_4 \cos\theta_2 \\ B &= 2r_1 r_4 \sin\theta_1 - 2r_2 r_4 \sin\theta_2 \\ C &= r_1^2 + r_2^2 + r_4^2 - r_3^2 - 2r_1 r_2(\cos\theta_1 \cos\theta_2 + \sin\theta_1 \sin\theta_2) \end{aligned} \tag{16}$$

$$\theta_4 = 2\tan^{-1}\left[\frac{-B + \sigma\sqrt{B^2 - C^2 + A^2}}{C - A}\right], \sigma = \pm \tag{17}$$

$$\theta_3 = \tan^{-1}\left[\frac{r_1 \sin\theta_1 + r_4 \sin\theta_4 - r_2 \sin\theta_2}{r_1 \cos\theta_1 + r_4 \cos\theta_4 - r_2 \cos\theta_2}\right] \tag{18}$$

$$\begin{aligned} \vec{r}_2 &= r_2(\cos\theta_2 i + \sin\theta_2 j) \\ \vec{r}_P &= \vec{r}_2 + \vec{r}_3 = r_2(\cos\theta_2 i + \sin\theta_2 j) + r_3(\cos\theta_3 i + \sin\theta_3 j) \\ &= \vec{r}_1 + \vec{r}_4 = r_1(\cos\theta_1 i + \sin\theta_1 j) + r_4(\cos\theta_4 i + \sin\theta_4 j) \\ &= \vec{r}_1 = r_1(\cos\theta_1 i + \sin\theta_1 j) \end{aligned} \tag{19}$$

Velocity:

$$\begin{bmatrix} -r_3\sin\theta_3 & r_4\sin\theta_4 \\ -r_3\cos\theta_3 & r_4\cos\theta_4 \end{bmatrix} \begin{Bmatrix} \dot{\theta}_3 \\ \dot{\theta}_4 \end{Bmatrix} = \begin{Bmatrix} r_2\dot{\theta}_2\sin\theta_2 \\ r_2\dot{\theta}_2\cos\theta_2 \end{Bmatrix} \tag{20}$$

$$\vec{r}_2 = r_2\dot{\theta}_2(-\sin\theta_2\, i + \cos\theta_2 j) \tag{21}$$

$$\vec{r}_P = r_4\dot{\theta}_4(-\sin\theta_4\, i + \cos\theta_4 j)$$

Acceleration:

$$\begin{bmatrix} -r_3\sin\theta_3 & r_4\sin\theta_4 \\ -r_3\cos\theta_3 & r_4\cos\theta_4 \end{bmatrix} \begin{Bmatrix} \ddot{\theta}_3 \\ \ddot{\theta}_4 \end{Bmatrix} = \tag{22}$$

$$\begin{Bmatrix} r_2\ddot{\theta}_2\sin\theta_2 + r_2\dot{\theta}_2^{\,2}\cos\theta_2 + r_3\dot{\theta}_3^{\,2}\cos\theta_3 - r_4\dot{\theta}_4^{\,2}\cos\theta_4 \\ r_2\ddot{\theta}_2\cos\theta_2 - r_2\dot{\theta}_2^{\,2}\sin\theta_2 - r_3\dot{\theta}_3^{\,2}\sin\theta_3 + r_4\dot{\theta}_4^{\,2}\sin\theta_4 \end{Bmatrix}$$

$$\vec{r}_2 = (-r_2\ddot{\theta}_2\sin\theta_2 - r_2\dot{\theta}_2^{\,2}\cos\theta_2)i + (r_2\ddot{\theta}_2\cos\theta_2 - r_2\dot{\theta}_2^{\,2}\sin\theta_2)j \tag{23}$$

$$\vec{r}_p = (-r_4\ddot{\theta}_4\sin\theta_4 - r_4\dot{\theta}_4^{\,2}\cos\theta_4)i + (r_4\ddot{\theta}_4\cos\theta_4 - r_4\dot{\theta}_4^{\,2}\sin\theta_4)j \tag{24}$$

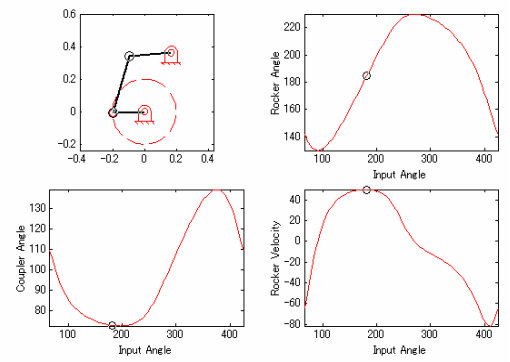

Fig. 8 Plot of the flapping wing kinematics.

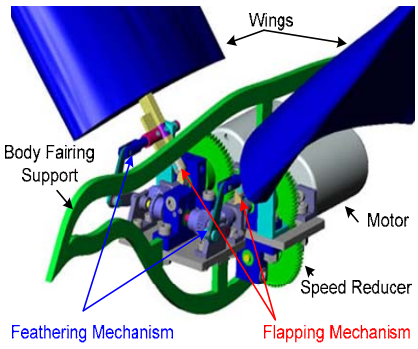

Fig. 9 The flapping-wing MAV model.

4.2 Twin-motor configuration

As shown in **Fig. 9**, the two identical sets of flapping-feathering mechanisms are connected to and driven by two identical Faulhaber™ coreless dc micromotors via two identical speed reducers. The right-hand side motor rotates in the clockwise direction, while the left-hand side motor rotates in the opposite direction (counter-clockwise). The speed reducer gear ratio is 16:1 and ensures sufficient torque transmission for the flapping-feathering mechanism to be able to move the wing over the design range.

The flight dynamics and controls of the flapping-wing MAV would be very interesting due to the fact that it has two independent motors; one motor in each wing. As an example, aside from

controlling the MAV by changing the angle of attack of the wings while in gliding by stopping and changing the positions of the motors, the MAV can also be controlled by varying the speed of the individual motor, thus producing asymmetric turning forces which is ideal for high speed maneuvering. This flight control method is inherent to pigeons, where pigeons, unlike other birds, use downstroke velocity asymmetries rather than angle of attack or surface area asymmetries, to produce the disparities in force needed for directional changes (Warrick et al[25]). To produce a bank for example, a velocity asymmetry is created early in the downstroke, and in the majority of cases, is then reversed at the end of the same downstroke, thus arresting the rolling angular momentum. Thus, a pigeon creates a precise average body position (e.g. bank angle) and flight path by producing a series of rapidly oscillating movements.

4.3 Design requirement parameters

The mechanical power requirement for a micro aerial vehicle of flapping-wing design can be computed by Eqs. (7) to (10) using the data listed in **Table 1** for steady level flight condition and the results obtained by the numerical simulations presented in Section 3. The design point parameters are therefore given as follows:

Mean Thrust, $\overline{T} = \frac{1}{2}\rho U^2 S C_T = 0.551\,N$

Lift, $L = W = 0.390\,kgf = 3.826\,N$

Drag, $D = \frac{1}{2}\rho U^2 S C_D = 0.331\,N$

Average Power, $\overline{P} = \overline{T}U \big/ \eta_P = 14.43\,W$.

In the computation, air at standard atmospheric pressure and temperature is being used, where $\rho = 1.225\ kg/m^3$ and $\nu = 1.46 \times 10^{-5}\ m^2/s$. Also, a value of $C_D = 0.072$ is being used in the computation for the drag coefficient of the pigeon's wings. The value of the average power needed to move the wings and to propel the vehicle at steady level flight condition is quite close to that of the estimated value for the total power given by Eq. (13). With the integration of the navigational and control system, the power requirement of the vehicle would eventually go even higher and exceed to that of the value given by Eq. (13).

The selection of suitable drive and transmission system is a major consideration in the vehicle's design for compactness and power sustainability. The required torque for each wing during its entire cycle should be constantly sustained by the driving motor. It is assumed here that each wing supports half of the vehicle's total mass and that the aerodynamic force is concentrated and acting at a distance of $0.25m$ from the root of the wing. The required torque per wing is therefore given below as,

$$\Gamma_{req} = \frac{390\,g}{2} \times 25\,cm = 4875\,g \cdot cm = 47.82\,mN \cdot m.$$

A suitable and efficient power transmission is therefore necessary for the driving motor to effectively move the wing to its desired kinematics.

5. Preliminary Experimentation

Not only the wings, but also the tail and the aerodynamic body fairing covering the flapping-feathering mechanism were shaped and patterned after the typical pigeon as listed in **Table 1**, and in Refs. 23) and 26). The flapping-wing MAV model was mounted at the Kyushu University Flutter Wind Tunnel to determine the efficacy of the flapping–feathering mechanism being employed and for the experimentation of its aerodynamic performance as shown in **Fig.10**.

The aerodynamic loads were measured by a six-component internal sting balance mounted inside the vehicle. This internal force balance was also constructed in accordance with the future measurements of the aerodynamic performance of the flapping-wing MAV being developed. Calibration was performed by loading the balance with calibrated forces. The signals of the balance are evaluated as a "calibration matrix", which gave a set of equations for "signals as functions of loads". The inverse version of this set of equations, "loads as functions of signals", was used to evaluate the balance signals recorded during experiments in the wind tunnel. The strain gage signals from the internal force balance were conditioned and recorded by a National Instruments™ DAQCard-6036E data acquisition card connected to a portable computer running LabVIEW™ 7.1 software as shown in **Fig.11**.

Fig. 10 The flapping-wing MAV model.

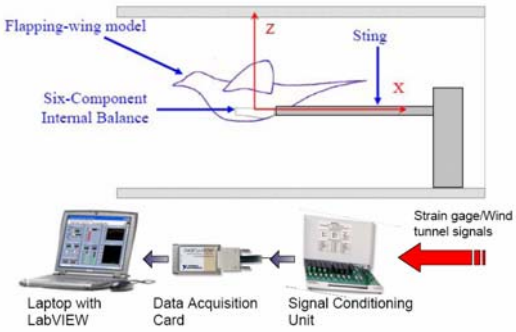

Fig. 11 The experimental set-up.

As a first step, the model was allowed to move and flap its wings with zero wind tunnel speed at different flapping frequencies but not above *3.5 Hz*. The MAV was then allowed to move and flap its wings at different flapping frequencies and wind tunnel air speeds. The maximum flapping frequency was set at *3.5 Hz*, while the maximum wind tunnel air speed was set at around *5 m/s*.

6. Conclusions and Future Works

A working flapping-wing micro aerial vehicle (MAV) that was shaped and patterned after a typical pigeon which utilized both flapping and feathering motions in its wings was successfully constructed and awaiting for a comprehensive performance evaluation and testing. The flapping-feathering mechanism being employed in this flapping-wing MAV model had well simulated the properly coordinated flapping and feathering motions in flapping flight with a phase angle difference of 90^{o}. Also, the flapping-wing MAV model had shown promising results during the preliminary testing. Since this model is employing both flapping and feathering motions in its wings, it is hoped that this type of flapping-wing model would exhibit far better aerodynamic performance than the existing fixed-wing and rotary-winged micro aerial vehicles.

The next steps include the evaluation of the aerodynamic performance of the flapping-wing

MAV by conducting comprehensive wind tunnel experimentations and numerical simulations, and the integration of the navigation and control system of the flapping-wing micro aerial vehicle being developed.

References

1) U.M. Norberg, Vertebrate flight: mechanics, physiology, morphology, ecology, and evolution, Springer, New York, 1990.
2) C.J. Pennycuick, "Wingbeat frequency of birds in steady cruising flight: new data and improved predictions," *Journal of Experimental Biology*, Vol. 199, pp. 1613-1618, 1996.
3) C.J. Pennycuick, "Actual and optimum flight speeds: field data reassessed," *Journal of Experimental Biology*, Vol. 200, pp. 2355-2361, 1997.
4) M. Lighthill, *Mathematical biofluiddynamics*, Society for Industry and Applied Mathematics, Philadelphia, PA, 1975.
5) J.M.V. Rayner, "A vortex theory of animal flight. Part 1. The vortex wake of a hovering animal," *Journal of Fluid Mechanics*, Vol. 4, pp. 697-730, 1979.
6) J.M.V. Rayner, "A vortex theory of animal flight. Part 2. The forward flight of birds," *Journal of Fluid Mechanics*, Vol. 4, pp. 731-763, 1979.
7) C.P. Ellington, "The aerodynamics of hovering insect flight IV. Aerodynamic mechanisms," *Philo. Trans. of the Royal Society of London. Series B*, Vol. 305, pp. 79-113, 1984.
8) C.P. Ellington, "The aerodynamics of hovering insect flight V. A vortex theory," *Philo. Trans. of the Royal Society of London. Series B*, Vol. 305, pp. 115-144, 1984.
9) M.H. Dickinson, F.O. Lehmann, and S.P. Sane, "Wing rotation and the basis of insect flight," *Science*, Vol. 284, pp. 1954-1960, 1999.
10) K.D. Jones, and M.F. Platzer, "An Experimental and numerical investigation of flapping-wing propulsion," AIAA Paper 99-0995, 1999.
11) M.J.C. Smith, "Simulating moth wing aerodynamics: Towards the development of flapping-wing technology," AIAA Journal, Vol. 34, No. 7, pp. 1348-1355, 1996.
12) M.S. Vest, and J. Katz, "Aerodynamic study of a flapping-wing micro-UAV," *37th AIAA Aerospace Sciences Meeting*, Nevada, AIAA 99-0994, 1999.
13) K. Isogai, Y. Shinmoto, and Y. Watanabe, "Effects of dynamic stall on propulsive efficiency and thrust of flapping wing," *AIAA Journal*, Vol. 34, No. 10, pp. 1145-1151, 1999.
14) K. Isogai, "Numerical Simulation of Unsteady Viscous Flow Around a Flapping Wing," *Proc. of the 2nd Int'l. Conf. on Computational Fluid Dynamics*, pp. 701-706, 2002.
15) M.S. Vest, and J. Katz, "Aerodynamic study of a flapping-wing micro-UAV," *37th AIAA Aerospace Sciences Meeting*, Nevada, AIAA 99-0994, 1999.
16) Knoller R. Die Gesetzedes Luftwiderstandes. Flug-und Motortechnik (Wien), Vol. 3 (21), pp. 1-7, 1909.
17) Betz A. Ein Beitrag zur Erklaerung Segelfluges. Z Flugtech Motorluftschiffahrt, Vol. 3, pp. 269-272, 1912.
18) T. Weis-Fogh, "Quick estimates of flight fitness in hovering animals, including novel mechanisms for lift production," *Journal of Experimental Biology*, Vol. 56, pp. 70-104, 1973.
19) C.J. Pennycuick, *Animal Flight*, London, Edward Arnold, 1972.
20) J.M.V. Rayner, and R. Gordon, "Visualization and modeling of the wakes of flying birds: vortices, gaits and flapping flight," *Motion Systems*, edited by Nachtigall and A. Wieser, BIONA Report, Gustav Fischer Verlag, Stuttgart, Vol. 13, pp. 165-173, 1999.
21) C.J. Pennycuick, "A wind tunnel study of gliding flight in the pigeon Columba livia," *Journal of Experimental Biology*, Vol. 49, pp. 509-526, 1968.
22) M.S. Vest, and J. Katz, "Unsteady aerodynamic model of flapping wings," *AIAA Journal*, Vol. 34, pp. 1435-1440, 1996.
23) W. Nachtigall, and J. Wieser, J., "Zeitschrift fur verleichende Physiologie 52, pp. 333-346, 1966.
24) B.S. Baldwin, and H. Lomax, *AIAA Paper* 78-257, 1978.
25) D.R. Warrick, M.W. Bundle, and K.P. Dial, "Bird Maneuvering Flight: Blurred Bodies, Clear Heads," *Integ. And Comp. Biology*, Vol. 42, pp. 141-148, 2002.
26) F.B. Gil, *Ornithology*, W.H. Freedman, New York, 1990.